

Timescales of the chaos onset in the general relativistic Poynting-Robertson effect

Vittorio De Falco^{1,*} and William Borrelli^{2,†}

¹*Department of Mathematics and Applications “R. Caccioppoli”,
University of Naples Federico II, Via Cintia, 80126 Naples, Italy*

²*Dipartimento di Matematica e Fisica, Università Cattolica del Sacro Cuore,
Via dei Musei 41, 25121 Brescia, Italy*



(Received 6 April 2021; accepted 3 May 2021; published 7 June 2021)

It has been proven that the general relativistic Poynting-Robertson effect in the equatorial plane of the Kerr metric shows a chaotic behavior for a suitable range of parameters. As a further step, we calculate the timescale for the onset of chaos through the Lyapunov exponents, estimating how this trend impacts the observational dynamics. We conclude our analyses with a discussion on the possibility to observe this phenomenon in neutron star and black hole astrophysical sources.

DOI: [10.1103/PhysRevD.103.124012](https://doi.org/10.1103/PhysRevD.103.124012)

I. INTRODUCTION

The general relativistic Poynting-Robertson (PR) effect is a phenomenon occurring in high-energy astrophysics. The motion of accreting matter in the vicinity of compact objects, such as black holes (BHs) and neutron stars (NSs), is strongly affected by the gravitational field. In addition, there could be the presence of other perturbing effects responsible for altering the geodesic motion of the surrounding matter (e.g., magnetic fields, hydrodynamical and magneto-hydrodynamical processes).

The x-ray electromagnetic radiation produced by an emitting source located close to the compact object (e.g., very hot corona around supermassive BHs in active galactic nuclei, stellar mass BHs, and weakly magnetised NSs in x-ray binary systems [1–3], boundary layers around NSs or the NS surface itself [4,5], and thermonuclear flashes occurring in the outermost layers of accreting NSs [6]) can intercept the inflowing matter modifying its motion. Indeed, the radiation force acting on relatively small-sized matter elements, treated as pointlike particles, is composed by the radiation pressure (being opposite to the gravitational attraction) and the PR radiation drag force, originating when the test particle absorbs the incoming radiation and then reemits it isotropically in its rest frame [7–10]. The PR effect removes very efficiently energy and angular momentum from the affected test particle, thus configuring as a *dissipative and nonlinear dynamical system in GR*.

From a modeling perspective, there are different treatments of the general relativistic PR effect going from Schwarzschild and Kerr to also other spacetimes from the

two-dimensional (2D) [9–11] to the three-dimensional (3D) formulations [12–16]. The common feature of all models is the presence of the *critical hypersurface*, a region where gravitational and radiation forces balance and the test particle moves on it stably [10,17,18].

From a theoretical point of view, the general relativistic PR effect has been treated under a Lagrangian formalism, determining, for the first time in the GR literature, the analytical form of the Rayleigh potential [18–21].

There are also several high-energy astrophysical applications, like investigating the way in which type I x-ray bursts on the NS surface may induce an increased mass inflow rate in the inner edge of the accretion disk [22–24]; studies on the matter velocity field close to a slowly rotating NS as a result of the PR effect for different star luminosities [25–28]; modeling the photospheric expansion occurring during Eddington-luminosity x-ray bursts [29,30] and associated oscillations [31,32]; observational evidences for changes in the inner disk properties, possibly induced by the PR effect from high signal to noise observations of type I x-ray bursts [33–36]; diagnosing the presence of wormholes through the detection of metric changes occurring in strong field regimes around BHs through the PR critical hypersurfaces [37,38]; and the PR effect that can drive the dynamical evolution of unequal supermassive BHs coalescence in galactic nuclei [39].

Recently, it has been shown that the general relativistic PR effect in the equatorial plane of the Kerr metric shows chaotic dynamics for a suitable parameter range [40]. In this paper, we would like to explore the timescale of the chaos onset and check how these configurations influence the PR dynamics within the Lyapunov exponents theory.

The paper is organized as follows: In Sec. II, we briefly describe the general relativistic PR effect model and its

*vittorio.defalco@physics.cz

†william.borrelli@unicatt.it

equations of motion; in Sec. III, we calculate the Lyapunov exponents of the general relativistic PR effect; in Sec. IV, we discuss our results proposing some observational classes of astrophysical sources to detect the chaos in the PR dynamics and finally, draw the conclusions.

II. GENERAL RELATIVISTIC POYNTING-ROBERTSON EFFECT IN THE EQUATORIAL PLANE OF THE KERR METRIC

We consider a test particle orbiting in the equatorial plane, $\theta = \pi/2$, around a rotating compact object, whose outside spacetime is described by the Kerr metric. In geometrical units ($c = G = 1$), its line element, $ds^2 = g_{\alpha\beta}dx^\alpha dx^\beta$, in standard Boyer-Lindquist coordinates, is parametrized by the mass, M , and spin, a , as

$$ds^2 = \left(\frac{2M}{r} - 1\right)dt^2 - \frac{4aM}{r}dt d\varphi + \frac{r^2}{\Delta}dr^2 + \rho d\varphi^2, \quad (1)$$

where $\Delta = r^2 - 2Mr + a^2$, and $\rho = r^2 + a^2 + 2a^2M/r$.

We assume that the motion of the test particle is influenced by the x-ray electromagnetic radiation field coming from an emitting source located in the vicinity of the rotating compact object. Radiation is treated here as a field superimposed on the Kerr spacetime, located in the equatorial plane and constituted by a coherent flux of photons, propagating outward from the center of the radiation source. At each time instant, the test particle is hit by a photon, moving along null geodesics in the equatorial plane on the Kerr spacetime. The radiation field includes also the effects of nonzero angular momentum of the photon field, b , which would result from the rotation of the central radiation source and/or frame dragging due to the rotating compact object. Therefore, the photons can be emitted either radially, $b = 0$, or in any other direction, $b \neq 0$, in the equatorial plane. It is useful to introduce the parameter β , defined as the azimuthal angle of the photon four-momentum measured clockwise from the φ axis in the local zero angular momentum observer (ZAMO) frame, which is related to the photon angular momentum b through the formula [10],

$$\cos \beta = \frac{bN}{\sqrt{\rho}(1 + bN^\varphi)}, \quad (2)$$

where $\beta \in [0, 2\pi]$ and the functions N, N^φ read as

$$N = \sqrt{\frac{\Delta}{\rho}}, \quad N^\varphi = -\frac{2aM}{r\Delta}. \quad (3)$$

It is important to note that for $\sin \beta > 0$ ($\sin \beta < 0$), we are considering outgoing (ingoing) photons [10].

We assume that the interaction between the radiation field and the test particle occurs through coherent and

isotropic scattering in the test particle rest frame with Thomson cross section, $\sigma_T = 6.7 \times 10^{-25} \text{ cm}^2$. The relative luminosity of the radiation field is encoded in the parameter A , which can be written as $A/M = L_\infty/L_{\text{Edd}}$ [9], where L_∞ stays for the luminosity measured by an observer at infinity, and $L_{\text{Edd}} \simeq 1.26 \times 10^{38} (M/M_\odot) \text{ erg s}^{-1}$ represents the Eddington limiting luminosity.

The dynamical system describing the equatorial motion of the test particle influenced by the Kerr gravitational field, the radiation pressure, and the PR effect is governed by a set of four coupled and fully general relativistic ordinary differential equations of the first order. The first two equations describe the test particle motion in the ZAMO frame in terms of the local spatial velocity ν and its azimuthal angle α measured clockwise with respect to the φ axis in the ZAMO frame. The last two equations transform these ZAMO quantities into the radial r and angular φ velocities. The set of equations of motion in the Kerr metric reads as [9,10]

$$\begin{aligned} \frac{d\nu}{dt} = & -\frac{N \sin \alpha}{\gamma^2} [a(n)^{\hat{r}} + 2\nu \cos \alpha \theta(n)^{\hat{r}}_{\hat{\varphi}}] \\ & + A \frac{(1 + bN^\varphi) [\cos(\alpha - \beta) - \nu][1 - \nu \cos(\alpha - \beta)]}{\gamma N r \sqrt{\rho} |\sin \beta|}, \end{aligned} \quad (4)$$

$$\begin{aligned} \frac{d\alpha}{dt} = & -\frac{N \cos \alpha}{\nu} [a(n)^{\hat{r}} + 2\nu \cos \alpha \theta(n)^{\hat{r}}_{\hat{\varphi}} + \nu^2 k_{(\text{lie})}(n)^{\hat{r}}] \\ & + A \frac{(1 + bN^\varphi) [1 - \nu \cos(\alpha - \beta)] \sin(\beta - \alpha)}{\gamma N r \sqrt{\rho} \nu |\sin \beta|}, \end{aligned} \quad (5)$$

$$\frac{dr}{dt} = \frac{N\nu \sin \alpha}{\sqrt{g_{rr}}}, \quad (6)$$

$$\frac{d\varphi}{dt} = \frac{N\nu \cos \alpha}{\sqrt{g_{\varphi\varphi}}} - N^\varphi, \quad (7)$$

where $\gamma = 1/\sqrt{1 - \nu^2}$ is the Lorentz factor, and $a(n)^{\hat{r}}, \theta(n)^{\hat{r}}_{\hat{\varphi}}, k_{(\text{lie})}(n)^{\hat{r}}$ are the acceleration vector, the expansion tensor, and the relative Lie curvature tensor, respectively, whose explicitly expressions are [10]

$$a(n)^{\hat{r}} = \frac{M[(r^2 + a^2)^2 - 4a^2Mr]}{r^3 \rho \sqrt{\Delta}}, \quad (8)$$

$$\theta(n)^{\hat{r}}_{\hat{\varphi}} = \frac{-aM(3r^2 + a^2)}{r^3 \rho}, \quad (9)$$

$$k_{(\text{lie})}(n)^{\hat{r}} = \frac{-\sqrt{\Delta}(r^3 - a^2M)}{r^3 \rho}. \quad (10)$$

A. Critical hypersurface

The general relativistic PR effect model admits as a particular solution one where gravitational attraction, radiation pressure, and radiation drag force balance. This configuration defines a region, dubbed as *critical hypersurface*, describing a circular orbit in the equatorial plane, where the test particle moves on it stably with constant velocity [10,17]. Therefore, imposing $\nu = \nu_{\text{crit}}$, $\alpha = 0$, $r = r_{\text{crit}}$ in the equations of motion, we obtain $d\nu/dt = d\alpha/dt = dr/dt = 0$, which entails [10]

$$\nu_{\text{crit}} = \cos \beta, \quad (11)$$

$$a(n)^{\hat{r}} + 2\theta(n)^{\hat{\phi}}\nu_{\text{crit}} + k_{(\text{Lie})}(n)^{\hat{r}}\nu_{\text{crit}}^2 = \frac{A(1 + bN^{\phi})^2 \text{sgn}(\sin \beta)}{N^2 r \sqrt{\rho} \gamma_{\text{crit}}^3}. \quad (12)$$

The first equation gives the constant velocity of the test particle on the critical hypersurface, whereas the second solved implicitly in terms of r permits one to determine the radius of the critical hypersurface in terms of M , a , A , b .

III. LYAPUNOV EXPONENTS OF THE GENERAL RELATIVISTIC PR EFFECT

The theory of the Lyapunov exponents is a generalization of the linear stability theory for dynamical systems, which allows one to quantify the rate of separation of infinitesimally close trajectories. Roughly speaking, it relies on studying the asymptotic properties of the tangent map to the dynamical system, and this is usually achieved analyzing the linearized flow. We give a short account on the method, referring to [41,42] for more details.

We first quickly introduce the general framework, before describing the concrete situation we are interested in. Let Φ^t be a differentiable flow on an n -dimensional connected Riemannian manifold (\mathcal{M}, h) , where h is the metric on the manifold \mathcal{M}^1 and $d\Phi_x^t: T_x\mathcal{M} \rightarrow T_x\mathcal{M}$ the associated tangent map. Here, $T_x\mathcal{M}$ denotes the tangent space to \mathcal{M} at $x \in \mathcal{M}$. The Lyapunov exponents are associated with the evolution of tangent vectors to \mathcal{M} . Namely, given a nonzero $\mathbf{v} \in T_x\mathcal{M}$, they are defined as

$$\chi(x, \mathbf{v}) := \lim_{t \rightarrow +\infty} \frac{\ln \|d\Phi_x^t \mathbf{v}\|_h}{t}. \quad (13)$$

As \mathbf{v} varies in $T_x\mathcal{M}$, $\chi(x, \mathbf{v})$ takes $s \leq n$ distinct values $\nu_1(x) > \dots > \nu_s(x)$, with $s = s(x)$. Then, one can compute *all* the Lyapunov exponents, letting vary the vectors $\mathbf{v} \in T_x\mathcal{M}$ in Eq. (13). However, as explained in [41], in practical computations, a random choice of vectors always

leads to the *largest* Lyapunov exponent because the others have essentially zero probability to be obtained.

Let $\chi_i(x)$, with $\chi_1(x) \geq \dots \geq \chi_n(x)$, be the Lyapunov exponents at x counted with their multiplicity. The sum of the first $p \geq 1$ Lyapunov exponents can be computed choosing p vectors $\mathbf{v}_1, \dots, \mathbf{v}_p \in T_x\mathcal{M}$ and then evaluating the volume of the parallelepiped generated by the transformed vectors $d\Phi^t \mathbf{v}_1, \dots, d\Phi^t \mathbf{v}_p$ through the formula,

$$\lim_{t \rightarrow \infty} \frac{1}{t} \text{Vol}_h^p([d\Phi_x^t \mathbf{v}_1, \dots, d\Phi_x^t \mathbf{v}_p]) = \sum_{i=1}^p \chi_i(x). \quad (14)$$

As an example of the applicability of the above formula, let us suppose, for instance, we want to compute the second Lyapunov exponent, $\chi_2(x)$. The first one $\chi_1(x)$ is easily determined by randomly choosing a vector $\mathbf{v}_1 \in T_x\mathcal{M}$ and then employing Eq. (13). Therefore, now one needs to choose just another independent vector $\mathbf{v}_2 \in T_x\mathcal{M}$, compute the volume of the parallelepiped $[d\Phi^t \mathbf{v}_1, d\Phi^t \mathbf{v}_2]$, and finally, take the limit for $t \rightarrow \infty$:

$$\lim_{t \rightarrow \infty} \frac{1}{t} \text{Vol}_h^2([d\Phi_x^t \mathbf{v}_1, d\Phi_x^t \mathbf{v}_2]) = \chi_1(x) + \chi_2(x). \quad (15)$$

Subtracting from this sum the value of $\chi_1(x)$, one obtains $\chi_2(x)$. It is now evident how to iteratively apply this method for computing all the Lyapunov exponents $\chi_i(x)$. One simply needs to add each time a new independent vector $\mathbf{v}_i \in T_x\mathcal{M}$ and to use Eq. (14).

However, as clarified in [42], this procedure requires a careful implementation from a numerical point of view, as two main issues arise. First, randomly choosing $\mathbf{v} \in T_x\mathcal{M}$, $\|dT_x^t \mathbf{v}\|_h$, it exponentially increases as $t \rightarrow \infty$. Moreover, when at least two vectors are involved in (14), the angle between two of them can rapidly become too small to be numerically handled. In [42], the authors solve all these issues and then provide tests and examples illustrating their computational strategy.

The concrete setting we are considering are those dynamical systems governed by a set of ordinary differential equations of the following type:

$$\frac{dX_i(t)}{dt} = f_i(X_1(t), \dots, X_n(t)), \quad i = 1, \dots, n, \quad (16)$$

where f_i are supposed to be smooth functions for all $i = 1, \dots, n$, and t plays the role of the time. Let us assume that a time-dependent stationary solution $(X_1^*(t), \dots, X_n^*(t))$ exists for the dynamical system (16); i.e., $f_i(X_1^*(t), \dots, X_n^*(t)) = 0$ for all $i = 1, \dots, n$. Let us consider now a small perturbation around the stationary solution, i.e., $X_i(t) = X_i^*(t) + \delta X_i(t)$ for all $i = 1, \dots, n$, and thus linearize the dynamical system (16),

¹In Sec. III B 1, we will see that the spacetime $\mathcal{M} = \mathbb{R}^3$ and the metric h on \mathcal{M} is the usual Euclidean metric.

$$\frac{d(\delta X_i(t))}{dt} = \mathbb{A}_{ij}(t)\delta X_j(t), \quad i, j = 1, \dots, n, \quad (17)$$

where $\mathbb{A}_{ij}(t)$ is the *linear stability matrix* obtained as

$$\mathbb{A}_{ij}(t) = \left. \frac{\partial f_i}{\partial X_j} \right|_{X_i^*(t)}, \quad i, j = 1, \dots, n. \quad (18)$$

The solution of the linearized Eq. (17) is

$$\delta X_i(t) = L_{ij}(t)\delta X_j(0), \quad i, j = 1, \dots, n, \quad (19)$$

where the *evolution matrix* $L_{ij}(t)$ satisfies

$$\dot{L}_{ij}(t) = \mathbb{A}_{im}(t)L_{mj}(t), \quad i, j = 1, \dots, n, \quad (20)$$

and $L_{ij}(0) = \delta_{ij}$. We observe that, *a priori*, \mathbb{A}_{im} depends on the time t . In the special case where the stationary solution is independent from the time t , the Lyapunov exponents are simply the eigenvalues of the time-independent matrix \mathbb{A}_{ij} . Then, the *principal Lyapunov exponent* is the maximal eigenvalue of such a matrix.

A. Proprieties of the Lyapunov exponents

For *conservative* dynamical systems, the sum of all Lyapunov exponents is zero because a volume element in the phase space is conserved by the flow. Instead, if the dynamical system is dissipative, the sum of Lyapunov exponents is negative, as the volume element shrinks along a trajectory. Therefore, the Lyapunov exponents provide information concerning local expansion and contraction of phase space, thus formalizing the concept of stretching rate along different directions [43].

Positive Lyapunov exponents are a useful index of the *sensitive dependence on the initial conditions*² [44–48]. Therefore, they are usually taken as a possible indication of chaos provided that some other conditions are satisfied.³ Lyapunov exponents are used to characterize unstable orbits, along which, chaotic dynamics can develop. As an example, the instability of some circular orbits around a Schwarzschild BH can be quantified by a positive principle Lyapunov exponent, although the geodesics around a Schwarzschild BH are not chaotic [50]. If a dynamical system shows a positive principal Lyapunov exponent,

²A dynamical system shows sensitive dependence on the initial conditions if tiny perturbations on the initial conditions lead to significantly different future behaviors.

³The widely accepted definition of *chaos* is due to Robert L. Devaney, and it fulfils three proprieties [49]: (1) sensitive dependence on initial conditions, (2) topologically mixing (any given region or open set of the phase space eventually overlaps with any other given region in the phase space), and (3) the presence of a dense set of periodic orbits (every point in the dynamical real space is approached arbitrarily close by periodic orbits).

$\bar{\lambda} > 0$, it is possible to define the *Lyapunov time* $T_{\bar{\lambda}} = 1/\bar{\lambda}$. This is a characteristic timescale on which a dynamical system is unstable or chaotic and beyond which, our predictions break down [46,50,51].

Despite being helpful, Lyapunov exponents must be exploited with caution as they present some drawbacks, especially in GR theory, which can be summarized as:

- (i) *They vary from orbit to orbit*, not encoding the collective behavior of all orbits and not usually catching generic information [46]. In order to get true and appropriate values, they should be averaged over many different points on the same trajectory. Sometimes, it can occur that in such a mean process, they could return zero values when the considered orbits move in and out of unstable regions [52–54];
- (ii) *They depend on the chosen time coordinate*. Since time is relative in GR, the same happens also for the Lyapunov exponents. If this remark is not taken properly into account, it can bring to erroneous results. However, whenever a preferred time direction exists, the uncertainty of time can be eliminated. For example, in the Schwarzschild and Kerr spacetimes where a timelike Killing vector exists, the coordinate time of the observer at infinity reveals itself to be the most appropriate choice [50,51].

B. Application of the Lyapunov theory to the general relativistic PR effect

The general relativistic PR effect is *rotationally invariant* (independent from the azimuthal angle φ) and *autonomous* (does not explicitly depend on the time t). Therefore, Eqs. (4)–(6) represent the dynamical system to investigate. Defined as $X = (\nu, \alpha, r)$, the dynamical system can be written as $dX/dt = f(X)$. We linearly perturb it around the critical hypersurface $X_0 = (\nu_0, 0, r_0)$ (being a stationary solution, i.e., $f(X_0) = \mathbf{0}$), where ν_0 and r_0 can be determined by exploiting Eqs. (11) and (12). We consider the following perturbations:

$$\nu = \nu_0 + \varepsilon\nu_1, \quad \alpha = \varepsilon\alpha_1, \quad r = r_0 + \varepsilon r_1, \quad \varepsilon \ll 1, \quad (21)$$

also written as $X = X_0 + \varepsilon X_1$, with $X_1 = (\nu_1, \alpha_1, r_1)$.

The components of the linearized 3×3 matrix $\mathbb{A} = (df/dX)_{X=X_0}$ can be found in Table I, where we obtain the linearized dynamical system $dX_1/dt = \mathbb{A} \cdot X_1$.

As already explained, since the dynamical system is autonomous, the Lyapunov exponents coincide with the eigenvalues of the matrix \mathbb{A} , denoted as $\{\lambda_1, \lambda_2, \lambda_3\}$. The *characteristic eigenvalue equation* in terms of λ is

$$c_0 + c_1\lambda + c_2\lambda^2 - \lambda^3 = 0, \quad (22)$$

where

TABLE I. Explicit expressions of the coefficients of the linearized matrix \mathbb{A} , where $a_{ij} = \partial f_i / \partial X_j$. The quantities with subscript 0 mean that they are evaluated in ν_0, r_0 . They can be found also in the related *Mathematica* notebook [55].

Coefficient	Explicit expression
χ_1	$2aM\rho^3 r_0[2a^2 r_0(-8M^2 + Mr_0 + 6r_0^2) + a^4(4M + 3r_0) + r_0^4(9r_0 - 14M)]$
χ_2	$-3\rho_0^2[r_0^7(20a^2M^2 + 1) - Mr_0^6(32a^2M^2 + 5) + 2r_0^5(12a^4M^2 + a^2 + 3M^2) + a^2r_0^3(-16a^2M^4 + 4a^2M^2 + a^2 + 12M^2) - a^2Mr_0^2(5a^2 + 12M^2) + 10a^4M^2r_0 - 8a^2Mr_0^4 - 2a^6M]$
χ_3	$2aM\rho_0 r_0^2[-4Ma^2r_0^3(2a^2M^2 + 9) + r_0^6(44a^2M^2 + 3) - 18Mr_0^5(4a^2M^2 + 1) + 3r_0^4(16a^4M^2 + 3a^2 + 8M^2) + a^2r_0^3(4a^2M^2 + 9a^2 + 36M^2) - 2a^2Mr_0(8a^4M^2 + 9a^2 + 12M^2) + 3a^4(a^2 + 4M^2)]$
χ_4	$r_0[6a^4r_0^2(-2a^4M^2 + 12a^2M^4 + a^2 + 2M^2) + 4a^2r_0^4(-8a^4M^6 - 2a^4M^2 + 3a^2 + 12M^2) + 2a^2Mr_0^3(16a^6M^3 + 6a^4M^2 - 24a^2M^3 - 15a^2 - 4M^2) + 3r_0^8(1 - 16a^4M^4) + 2Mr_0^7(40a^4M^4 + 6a^2M^2 - 9) + 2r_0^6(-24a^6M^4 - 6a^4M^2 - 12a^2M^4 + 5a^2 + 18M^2) + 2Mr_0^5(8a^6M^4 + 24a^4M^2 - 21a^2 - 12M^2) - 6a^6Mr_0(4a^2M^2 + 1) + a^8]$
ξ_1	$-6aMr_0^2\rho_0^2(a^2 + 3r_0^2)$
ξ_2	$\rho_0[2r_0^5(18a^2M^2 - 1) + 3a^2r_0^3(4a^2M^2 - 1) + a^2r_0(6M^2 - a^2) - a^2Mr_0^2 - 2a^4M + 3Mr_0^4]$
ξ_3	$2aMr_0[3r_0^5(1 - 4a^2M^2) + a^2r_0^3(3 - 4a^2M^2) + 2a^2M^2r_0 - a^2Mr_0^2 - 2a^4M - 5Mr_0^4]$
ψ_1	$\nu_0^2[a^2(2M^2 - Mr_0 + r_0^2) + r_0^3(r_0 - 2M)] + M(2a^2(r_0 - 2M) + r_0^3)$
ψ_2	$2a^3bMr_0^3(-2M^2 + Mr_0 - 3r_0^2) + 4a^5bM^2r_0^2 + a^2r_0^4(-12M^2 + 2Mr_0 + 5r_0^2) + a^4r_0(2M + r_0)(-6M^2 + Mr_0 + 4r_0^2) + a^6(2M + r_0)^2 + 2abMr_0^6(5M - 3r_0) + r_0^7(2r_0 - 3M)$
ψ_3	$-2aM\nu_0[a^2r_0^3(12M^2 - 23Mr_0 + 17r_0^2) + 3a^6(M + r_0) - a^4r_0(M - r_0)(4M + 11r_0) + 3r_0^6(3r_0 - 7M)]$
ψ_4	$-M[2a^4r_0(2M^2 + 5Mr_0 - 4r_0^2) + a^2r_0^4(25M - 7r_0) - 3a^6(M + r_0) - 2r_0^7]$
ψ_5	$-a^2r_0^4(20M^2 - 9Mr_0 + r_0^2) + a^4Mr_0(-2M^2 - 5Mr_0 + 10r_0^2) + 3a^6M(M + r_0) + r_0^7(4M - r_0)$
a_{11}	$\frac{A\gamma_0(1-2\nu_0^2)[(\rho_0-2abMr_0)^2+b^2\Delta_0]-b\sqrt{\Delta_0}\nu_0(3\nu_0^2-1)(2abMr_0-\rho_0)}{r_0\sqrt{\Delta_0}\rho_0(2abMr_0-\rho_0)\sqrt{1-\frac{b^2\Delta_0}{(\rho_0-2abMr_0)^2}}}$
a_{12}	$\frac{A\gamma_0\sqrt{\rho_0}r_0^2[(\nu_0^2+1)(2abMr_0+\rho_0)-2b\sqrt{\Delta_0}\nu_0]-M[-4a^2Mr_0-2a\sqrt{\Delta_0}\nu_0(a^2+3r_0^2)+(a^2+r_0^2)^2]}{\sqrt{\Delta_0}\gamma_0^2\rho_0^{3/2}r_0^3}$
a_{13}	$-A\frac{\{b\Delta_0^{3/2}(\nu_0^2+1)[b^3\xi_3+b^2\xi_2+b\xi_1+\rho_0^3r_0(a^2+3r_0^2)]+\nu_0(b^4\chi_4+b^3\chi_3+b^2\chi_2+b\chi_1-r_0\rho^6)\}}{\gamma_0\Delta_0^{3/2}\rho_0^2r_0^3\left(1-\frac{b^2\Delta_0}{(\rho_0-2abMr_0)^2}\right)^{3/2}}$
a_{21}	$\frac{\sqrt{\Delta_0}(a^4M+\gamma_0^2r_0\psi_1)-A\gamma_0\sqrt{\rho_0}(-2abMr_0-b\sqrt{\Delta_0}\nu_0^2+\rho)}{\sqrt{\Delta_0}\rho^{3/2}r_0^2\nu_0^2}$
a_{22}	$A\frac{\nu_0[(\rho-2abMr_0)^2-2b^2\Delta_0]+b\sqrt{\Delta_0}(\rho_0-2abMr_0)}{\gamma_0\sqrt{\Delta_0}\rho_0r_0\nu_0(2abMr_0-\rho_0)\sqrt{1-\frac{b^2\Delta_0}{(\rho-2abMr_0)^2}+1}}$
a_{23}	$-\frac{A\sqrt{\rho_0}r_0[\psi_2-b\Delta_0^{3/2}r_0^2\nu_0(a^2+3r_0^2)]-\gamma_0\Delta_0M[\sqrt{\Delta_0}(\nu_0^2\psi_5+\psi_4)+\psi_3]}{\gamma_0\Delta_0^{3/2}\rho_0^{5/2}r_0^5\nu_0}$
a_{32}	$\frac{\Delta_0\nu_0}{\sqrt{\rho_0}r_0}$
$a_{31} = a_{33}$	0

$$c_0 = \det \mathbb{A}, \quad c_2 = \text{Tr} \mathbb{A},$$

$$c_1 = \sum_{\substack{i,j=1 \\ i \neq j}}^3 \left(\frac{a_{ij}a_{ji} - a_{ii}a_{jj}}{2} \right). \quad (23)$$

Since the eigenvalues are the zeroes of a polynomial of third order, we can analytically determine them [56].

1. Lyapunov and PR timescales

We can calculate the Lyapunov timescale for the chaos onset as $T_{\bar{\lambda}} = 1/\bar{\lambda}$, where $\bar{\lambda}$ is the principal Lyapunov exponent. This time must be compared with the PR timescale T_{PR} , defined as the time from the start of the numerical simulation until the test particle reaches, for the first time, the critical hypersurface for moving then on that

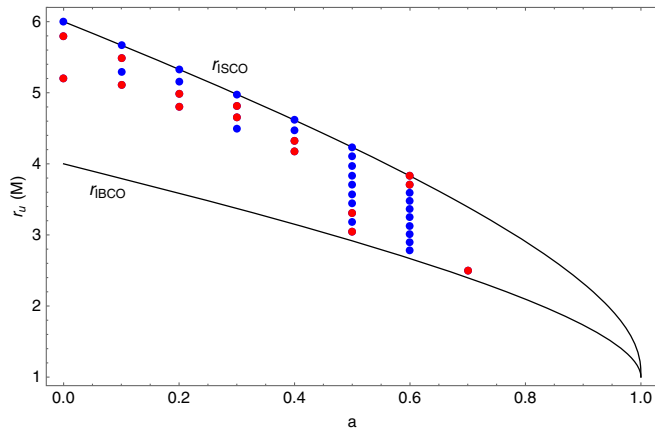


FIG. 1. Parameter space (r_u, a, b) , where r_u is the homoclinic orbit's parameter, and b is fixed to $b = 3$. This space is delimited by the innermost bound circular orbit, r_{IBCO} , and the innermost stable circular orbit, r_{ISCO} . All the (blue and red) dots represent the parameter subspace, in correspondence of which the chaotic dynamic occurs. The red dots are the selected examples reported in simulations 1–15 in Table II.

stably.⁴ This time is calculated numerically for each simulation. In order to understand whether the chaotic behavior is influential on the global PR dynamics, we compute the ratio $T_{\bar{\lambda}}/T_{\text{PR}}$, and if it is smaller (greater) than one, then the chaos is important (unimportant) [51].

As examples, we consider selected data from our previous numerical simulations; see Fig. 1 (see also Fig. 7 in Ref. [40], for comparison). The specific data for these simulations are reported in Table II; see simulations 1–15. We added also other five examples not reported in previous studies in order to show some variability of parameters; see simulations 16–20 in Table II.

IV. DISCUSSIONS AND CONCLUSIONS

The strategy to detect chaos in the PR dynamics relies on computing the *Melnikov integral* \mathcal{M} , whose integrating function is the Poisson brackets of the unperturbed Kerr Hamiltonian function and the PR dissipative perturbations. This is a function of mass M , spin a , homoclinic orbit parameter r_u , photon impact parameter b , and the test particle's initial condition r_0 , i.e., $\mathcal{M} = \mathcal{M}(M, a, r_u, b; r_0)$ [40]. If there is a combination of these parameters that nullifies \mathcal{M} , this means that, in correspondence of these values, chaotic dynamics occurs. The general relativistic PR effect shows chaos for a suitable range of parameters; see Fig. 1 for an example.⁵

⁴There are some examples where the test particle can cross the critical hypersurface and then not move anymore on that (see Figs. in Sec. 3.4 of Ref. [57], for more details).

⁵For discovering other ranges of parameters for which chaos occurs, we developed a code written in *Mathematica*, which permits one to facilitate this research (see Ref. [47] in [40], for more details).

As subsequent analysis, in this work, we have investigated whether the chaotic dynamics is observationally relevant on the PR dynamics. To this end, we have exploited the theory of Lyapunov exponents, which allows one to estimate the timescale of the chaos onset. The procedure is essentially based on perturbing the general relativistic PR equations of motion (4)–(6) for low luminosities in terms of the parameter $\varepsilon = A/M \ll 1$ around the critical hypersurface values (configuration of equilibrium for the PR dynamical system); see Eq. (21). Therefore, after performing these calculations, we obtain the linearized matrix \mathbb{A} , which is numerically determined once M, a, A, b, r_0 have been assigned. Since the PR model is an autonomous dynamical system, the eigenvalues of \mathbb{A} are exactly the *Lyapunov exponents* $\{\lambda_1, \lambda_2, \lambda_3\}$. Finally, considering the maximum of the real parts of the eigenvalues, we determine the *principal Lyapunov exponent* $\bar{\lambda}$, whose inverse value corresponds to the *Lyapunov timescale* $T_{\bar{\lambda}} = 1/\bar{\lambda}$ for estimating the chaos onset. Another fundamental information is encoded in the PR timescale T_{PR} , defined as the time from the start of the numerical simulation until the test particle reaches, for the first time, the critical hypersurface for then moving on it stably. In order to understand how the chaotic behavior impacts the PR dynamics, we consider the ratio between the Lyapunov $T_{\bar{\lambda}}$ and PR T_{PR} timescales: If $T_{\bar{\lambda}}/T_{\text{PR}} \leq 1$, it means that the chaos is observationally significant, whereas if $T_{\bar{\lambda}}/T_{\text{PR}} > 1$, it is unimportant.

We performed 20 numerical simulations, whose detailed values are reported in Table II. We note that the chaos is significant for simulations 7–20, while there is any influence for simulations 1–6. However, we checked by performing other numerical simulations that varying the luminosity parameter A , namely making it smaller and smaller, it is possible to have also for simulations 1–6 a ratio lower than one. Once we calculate the Lyapunov timescale, we have an indication on how to tune the parameters for having a PR timescale such that it is smaller or greater than the time for the chaos onset. We note also that when we fixed the value of the photon impact parameter b , and chosen, for hypothesis, a small value of the luminosity parameter A , it follows that an important role is played by the spin a . Indeed, the test particle's initial conditions are also fundamental, but they are strongly related to $\{M, a, b\}$ via the Melnikov integral \mathcal{M} [40].

From an observational point of view, it is significant to understand how to identify the astrophysical systems where chaos in the PR dynamics can be detected. The requirement of low luminosities permits one to provide a first stringent criterion. The mass M and spin a of a compact object can be normally estimated by means of several strategies (see e.g., [58,59], for more details). In addition, the surrounding accreting matter can be found distributed almost everywhere with generally different velocities, including some initial configurations for having chaotic dynamics [60].

TABLE II. Numerical simulations performed using as test particle's initial conditions (r_p, α_p, ν_p) and the PR effect model parameters b, A, a , together with the critical hypersurface radius r_0 . As a result, we obtain the Lyapunov timescale T_λ , the PR timescale T_{PR} , and the ratio between these two times in order to see whether the PR effect is important [55].

SIM. #	ν_p	α_p	r_p (M)	b (M)	A	a	r_0 (M)	T_λ (M)	T_{PR} (M)	T_λ/T_{PR}
1	0.82	0.52	2.84	3	0.0001	0	2.00	7.97×10^6	178703.57	44.59
2	0.72	0.30	3.51	3	0.0001	0	2.00	7.97×10^6	178703.57	43.60
3	0.89	0.76	2.39	3	0.001	0.1	1.9950	587441.09	47363.77	12.40
4	0.92	0.91	2.25	3	0.001	0.1	1.9950	587441.09	47397.65	12.39
5	0.79	0.45	2.80	3	0.01	0.2	1.9800	14352.60	5164.82	2.78
6	0.75	0.35	3.03	3	0.01	0.2	1.9800	14352.60	5187.24	2.77
7	0.75	0.34	2.92	3	0.01	0.3	1.9541	2470.75	5347.96	0.46
8	0.73	0.29	3.06	3	0.01	0.3	1.9541	2470.75	5350.97	0.46
9	0.77	0.36	2.70	3	0.01	0.4	1.9167	15.79	5558.25	2.84×10^{-3}
10	0.73	0.29	2.88	3	0.01	0.4	1.9167	15.79	5583.53	2.83×10^{-3}
11	0.29	0.73	14.31	3	0.1	0.5	4.55	24.14	3397.87	7.10×10^3
12	0.40	0.33	7.35	3	0.1	0.5	4.55	24.14	2691.15	0.01
13	0.62	0.04	3.37	3	0.1	0.6	5.62	213.32	3733.26	0.06
14	0.62	0.03	3.42	3	0.1	0.6	5.62	213.32	3727.37	0.06
15	0.14	0.24	21.31	3	0.1	0.7	6.16	264.20	264.20	0.06
16	0.70	0.22	3.29	3.1	0.1	0.3	1.9698	4.83	1029.39	4.69×10^{-3}
17	0.67	0.11	3.17	3.1	0.1	0.5	5.88	619.76	4193.14	0.15
18	0.63	0.03	3.61	3.2	0.1	0.5	6.82	557.15	5227.02	0.11
19	0.61	0.05	4.03	3.3	0.1	0.4	7.22	415.77	5608.68	0.07
20	0.60	0.05	4.36	3.4	0.1	0.3	7.66	499.52	6182.17	0.08

Therefore, only the photon impact parameter b must be estimated. It cannot be measured directly from the observational data, but it can be linked to the emitting surface radius R_\star (supposed to be a spherical region) and angular velocity Ω_\star (assuming that the emitting surface rigidly rotates) through the formula (see Ref. [13], for more details),

$$b \equiv \left[-\frac{g_{t\varphi} + g_{\varphi\varphi}\Omega_\star}{g_{tt} + g_{t\varphi}\Omega_\star} \right]_{r=R_\star} = \frac{a^2 R_\star \Omega_\star \rho(R_\star)}{R_\star + 2M(a\Omega_\star - 1)}. \quad (24)$$

In addition, we have that $\Omega_\star \in [\Omega_-, \Omega_+]$, being

$$\Omega_\pm = \frac{-g_{t\varphi} \pm \sqrt{g_{t\varphi}^2 - g_{tt}g_{\varphi\varphi}}}{g_{\varphi\varphi}}. \quad (25)$$

Since R_\star can be estimated from the observations, we can relate Ω_\star in terms of b, a, M, R_\star , via Eq. (24), as

$$\Omega_\star = \frac{2aM + b(R_\star - 2M)}{\rho(R_\star) - 2Mab}. \quad (26)$$

The last condition thus imposes a further constraint to single out the astrophysical systems exhibiting chaos.

It is important now to distinguish the physics of BH and NS systems. For a *standard NS* of mass $M = 1.4 M_\odot$ and radius $R_\star = 6M$, if we consider the NS surface as emitting

region, then the spin a can be expressed as a function of the NS angular velocity Ω_\star through $a = C\Omega_\star/z$, where C depends on the NS structure and equation of state, which in our case, amounts to be $C = 1.1 \times 10^{-4}$ s/rad [61], and $z = (1.4GM_\odot/c^3)/(2\pi)$ is the conversion gravitational factor. In this way, we have $a = a(b)$, which for $b \sim 3$, we obtain $a \sim 10^{-6}$, corresponding thus to extremely slowly rotating NSs, namely $\Omega_\star \sim 0.06$ rad/s or spin period $T_\star \equiv 2\pi/\Omega_\star \sim 100$ s. In Fig. 2, we plot how the NS angular velocity Ω_\star and spin period T_\star changes in terms of the photon impact parameter b . In addition, since NSs are very small compact objects, they have a very low

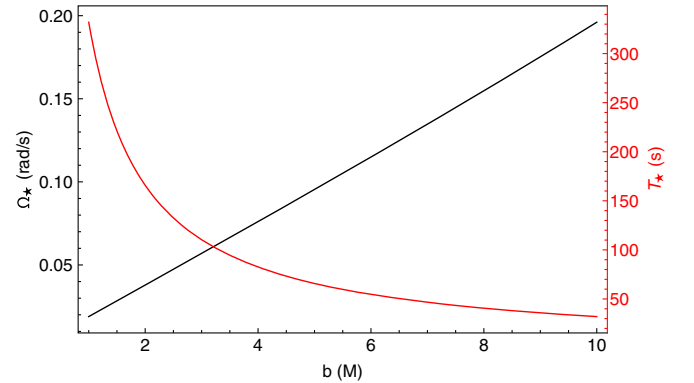


FIG. 2. Plot of the NS surface's angular velocity Ω_\star and spin period T_\star in terms of photon impact parameter b .

TABLE III. Information about six examples (ex.) of some astrophysical sources divided in three types analysed in Sec. IV.

Type	EX. #	SOURCE id.	M (M_{\odot})	R_{\star} (M)	T_{\star} (s)	A	Ref.
NS surface	1	A0535 + 26	1.50	4.52	103.00	4.46×10^{-6}	[62]
	2	GX 1 + 4	1.35	5.03	121.00	4.46×10^{-6}	[63]
	3	Vela X-1	1.88	3.61	283.00	4.46×10^{-6}	[64]
Boundary layer around a NS	4	GX 3 + 1	1.40	6.67	0.74×10^{-3}	0.058	[65]
	5	4U 1702-429	1.40	5.35	0.53×10^{-3}	0.058	[65]
	6	GX 301-2	1.40	5.36	0.54×10^{-3}	0.058	[65]
Hot corona around a BH ^a	7	NGC 5506	10^8	10.00	1.01×10^{-3}	0.002	[1]
	8	MCG-6-30-15	0.18×10^{-3}	2.90	0.07	0.03	[1]
	9	Cyg A	2.51×10^9	10.00	1.01×10^{-3}	0.003	[1]

^aThe sources we have chosen have all extreme spin values, namely $0.95 < a < 1$.

luminosity. Assuming that the NS surface temperature is $T = 10^6$ K, its luminosity can be calculated through the Stefan-Boltzmann law in terms of the Sun's luminosity (where Sun's temperature $T_{\odot} = 5800$ K and radius $R_{\odot} = 7 \times 10^5$ Km), thus obtaining $L/L_{\odot} = 0.2$. The Eddington luminosity is $L_{\text{Edd}} = 4.48 \times 10^4 L_{\odot}$; therefore, $A \leq 4.46 \times 10^{-6}$. In rows 1, 2, and 3 in Table III, we report the data of some NSs, in which our study can be applied.

Instead, if we consider either a boundary layer around a NS or a hot corona around a BH, a and Ω_{\star} are now independent. In the case of a *boundary layer around a NS*, we know that it is located very close to the NS surface, $R_{\star} \sim (5 - 7)M$, and it is rigidly rotating with Keplerian angular velocity $\Omega_{\star} = \Omega_K(R_{\star}) \equiv M/(a + R_{\star})^{3/2}$ [5]. The additional requirement of low luminosities sees these configurations hosted in atoll sources, characterized by $A \lesssim 0.06$ [65]. In Fig. 3, we plot the photon impact parameter b in terms of the NS spin a , the only free parameter in this case. Finally in rows 3, 4, and 5 in Table III, there are the data of some astrophysical examples.

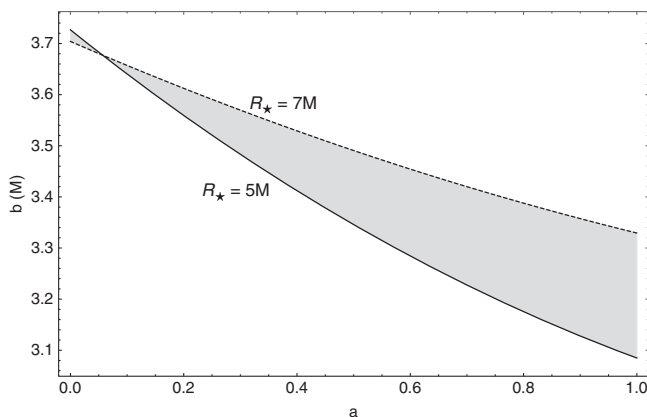


FIG. 3. Plot of the NS boundary layer's photon impact parameter b in terms of the NS spin a . The continuous ($R_{\star} = 5M$) and dashed ($R_{\star} = 7M$) lines delimit the light grey shaded area, which includes all admissible physical cases.

In the BH case, the emitting surface is represented by the hot corona, which is located in the range of $R_{\star} \sim (3 - 10)M$. We assume that the matter is rotating with Keplerian velocity $\Omega_{\star} = \Omega_K(R_{\star})$. There are, however, different models of the hot corona's angular velocity proposed in the literature (see Ref. [66], for more details). We impose also that these sources must be characterized by very small luminosities $A \lesssim 0.01$. In Fig. 4, we plot the photon impact parameter b in terms of the BH spin values using different models of the hot corona's angular velocity as reported in Ref. [66], in order to show how the b range values change in terms of different approaches. In rows 7, 8, and 9 in Table III, we show the data of some astrophysical sources.

The above discussions, together with the related formulas, plots, and examples, provide some basic strategies,

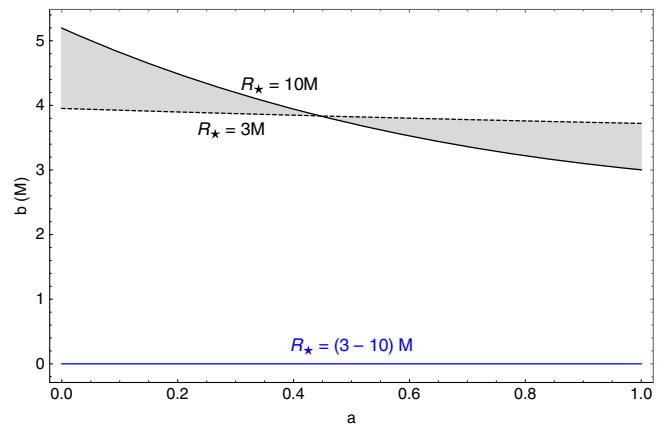


FIG. 4. Plot of the BH hot corona's photon impact parameter b in terms of the BH spin a for different locations (light gray shaded area), delimited by $R_{\star} = 3M$ (continuous line) and $R_{\star} = 10M$ (dashed line) in terms of different models of angular velocity Ω_{\star} : Keplerian $\Omega_K(R_{\star})$ coincident with the slablike in the equatorial plane (black lines) and ZAMO $\Omega_{\text{ZAMO}} = [-g_{t\varphi}/g_{\varphi\varphi}]_{r=R_{\star}}$ (blue line). Looking at Eq. (24), it is understandable why to Ω_{ZAMO} corresponds always to $b = 0$ for all possible values of a and R_{\star} .

which could be more extensively investigated and improved from an observational point of view through the analysis of several data related to astrophysical BH and NS sources. In addition, our approach is not only restricted to the PR effect, but it can be further extended to study the timescales of other relevant phenomena occurring in high-energy accretion physics (see e.g., [67–70]).

ACKNOWLEDGMENTS

V. D. F. thanks Gruppo Nazionale di Fisica Matematica of Istituto Nazionale di Alta Matematica for support. W. B. acknowledges support from Gruppo Nazionale per l'Analisi Matematica, la Probabilità e le loro Applicazioni of Istituto Nazionale di Alta Matematica.

-
- [1] A. C. Fabian, A. Lohfink, E. Kara, M. L. Parker, R. Vasudevan, and C. S. Reynolds, *Mon. Not. R. Astron. Soc.* **451**, 4375 (2015).
- [2] R. C. Reis and J. M. Miller, *Astrophys. J. Lett.* **769**, L7 (2013).
- [3] C. Done, M. Gierliński, and A. Kubota, *Astron. Astrophys. Rev.* **15**, 1 (2007).
- [4] N. A. Inogamov and R. A. Sunyaev, *Astron. Lett.* **25**, 269 (1999), <http://adsabs.harvard.edu/abs/1999AstL...25..269I>.
- [5] R. Popham and R. Sunyaev, *Astrophys. J.* **547**, 355 (2001).
- [6] W. H. G. Lewin, J. van Paradijs, and R. E. Taam, *Space Sci. Rev.* **62**, 223 (1993).
- [7] J. H. Poynting, *Mon. Not. R. Astron. Soc.* **64**, 1 (1903).
- [8] H. P. Robertson, *Mon. Not. R. Astron. Soc.* **97**, 423 (1937).
- [9] D. Bini, R. T. Jantzen, and L. Stella, *Classical Quantum Gravity* **26**, 055009 (2009).
- [10] D. Bini, A. Geralico, R. T. Jantzen, O. Semerák, and L. Stella, *Classical Quantum Gravity* **28**, 035008 (2011).
- [11] D. Bini, A. Geralico, and A. Passamonti, *Mon. Not. R. Astron. Soc.* **446**, 65 (2015).
- [12] V. De Falco, P. Bakala, E. Battista, D. Lančová, M. Falanga, and L. Stella, *Phys. Rev. D* **99**, 023014 (2019).
- [13] P. Bakala, V. De Falco, E. Battista, K. Goluchová, D. Lančová, M. Falanga, and L. Stella, *Phys. Rev. D* **100**, 104053 (2019).
- [14] M. Wielgus, *Mon. Not. R. Astron. Soc.* **488**, 4937 (2019).
- [15] V. De Falco, P. Bakala, and M. Falanga, *Phys. Rev. D* **101**, 124031 (2020).
- [16] V. De Falco and M. Wielgus, *Phys. Rev. D* **103**, 084056 (2021).
- [17] V. De Falco and P. Bakala, *Phys. Rev. D* **101**, 024025 (2020).
- [18] V. De Falco, *Emerging Sci. J.* **4**, 214 (2020).
- [19] V. De Falco, E. Battista, and M. Falanga, *Phys. Rev. D* **97**, 084048 (2018).
- [20] V. De Falco and E. Battista, *Europhys. Lett.* **127**, 30006 (2019).
- [21] V. De Falco and E. Battista, *Phys. Rev. D* **101**, 064040 (2020).
- [22] M. A. Walker, *Astrophys. J.* **385**, 642 (1992).
- [23] D. Lančová, P. Bakala, K. Goluchová, M. Falanga, V. De Falco, and L. Stella, in *Proceedings of RAGtime 17-19: Workshops on Black Holes and Neutron Stars, 17-19/23-26 Oct., 1-5 Nov. 2015/2016/2017, Opava, Czech Republic*, edited by Z. Stuchlík, G. Török, and V. Karas (Silesian University, Opava, 2017), pp. 127–136, ISBN 978-80-7510-257-7, ISSN 2336-5676.
- [24] P. C. Fragile, D. R. Ballantyne, and A. Blankenship, *Nat. Astron.* **4**, 541 (2020).
- [25] M. A. Abramowicz, G. F. R. Ellis, and A. Lanza, *Astrophys. J.* **361**, 470 (1990).
- [26] F. K. Lamb and M. C. Miller, *Astrophys. J.* **439**, 828 (1995).
- [27] M. C. Miller and F. K. Lamb, *Astrophys. J.* **470**, 1033 (1996).
- [28] M. C. Miller, F. K. Lamb, and D. Psaltis, *Astrophys. J.* **508**, 791 (1998).
- [29] M. Wielgus, W. Kluźniak, A. Sadowski, R. Narayan, and M. Abramowicz, *Mon. Not. R. Astron. Soc.* **454**, 3766 (2015).
- [30] M. Wielgus, in *Star Clusters and Black Holes in Galaxies across Cosmic Time*, edited by Y. Meiron, S. Li, F.-K. Liu, and R. Spurzem, IAU Symposium Vol. 312 (2016), pp. 131–134, <https://doi.org/10.1017/S1743921315007693>.
- [31] M. Wielgus, A. Stahl, M. Abramowicz, and W. Kluźniak, *Astron. Astrophys.* **545**, A123 (2012).
- [32] D. A. Bollimpalli, M. Wielgus, D. Abarca, and W. Kluźniak, *Mon. Not. R. Astron. Soc.* **487**, 5129 (2019).
- [33] D. R. Ballantyne and T. E. Strohmayer, *Astrophys. J. Lett.* **602**, L105 (2004).
- [34] L. Keek, D. R. Ballantyne, E. Kuulkers, and T. E. Strohmayer, *Astrophys. J.* **789**, 121 (2014).
- [35] L. Keek, D. R. Ballantyne, E. Kuulkers, and T. E. Strohmayer, *Astrophys. J. Lett.* **797**, L23 (2014).
- [36] L. Keek *et al.*, *Astrophys. J. Lett.* **855**, L4 (2018).
- [37] V. De Falco, E. Battista, S. Capozziello, and M. De Laurentis, *Phys. Rev. D* **101**, 104037 (2020).
- [38] V. De Falco, E. Battista, S. Capozziello, and M. De Laurentis, *Phys. Rev. D* **103**, 044007 (2021).
- [39] X. Chen, D. N. C. Lin, and X. Zhang, *Astrophys. J. Lett.* **893**, L15 (2020).
- [40] V. De Falco and W. Borrelli, *Phys. Rev. D* **103**, 064014 (2021).
- [41] G. Benettin, L. Galgani, A. Giorgilli, and J.-M. Strelcyn, *Meccanica* **15**, 9 (1980).
- [42] G. Benettin, L. Galgani, A. Giorgilli, and J.-M. Strelcyn, *Meccanica* **15**, 21 (1980).
- [43] H. D. Abarbanel, M. I. Rabinovich, and M. M. Sushchik, *Introduction to Nonlinear Dynamics for Physicists*, Vol. 53 (World Scientific, Singapore, 1993).
- [44] S. Wiggins, *Global Bifurcations and Chaos: Analytical Methods*, Applied Mathematical Sciences Series V. 73 (Springer-Verlag, New York, 1988).

- [45] M. Tabor, *Chaos and Integrability in Nonlinear Dynamics: An Introduction*, Wiley-Interscience publication (Wiley, New York, 1989).
- [46] S. H. Strogatz, *Nonlinear Dynamics and Chaos: With Applications to Physics, Biology, Chemistry and Engineering* (Westview Press, 2000), <https://www.bibsonomy.org/bibtex/2e3b3dc5a68df87d71becbe75709a7121/richterek>.
- [47] E. Ott, *Chaos in Dynamical Systems* (Cambridge University Press, Cambridge, England, 2002).
- [48] J. Guckenheimer and P. Holmes, *Nonlinear Oscillations, Dynamical Systems, and Bifurcations of Vector Fields*, Applied Mathematical Sciences (Springer, New York, 2002).
- [49] R. Devaney, *An Introduction to Chaotic Dynamical Systems* (CRC Press, 2018).
- [50] N. J. Cornish, *Phys. Rev. D* **64**, 084011 (2001).
- [51] N. J. Cornish and J. Levin, *Classical Quantum Gravity* **20**, 1649 (2003).
- [52] J. D. Barrow, *Phys. Rev. Lett.* **46**, 963 (1981).
- [53] J. D. Barrow, *Phys. Rep.* **85**, 1 (1982).
- [54] D. Hobill, A. Burd, and A. Coley, *Deterministic Chaos in General Relativity*, Nato Science Series B: (Springer US, New York, 1994).
- [55] See Supplemental Material at <http://link.aps.org/supplemental/10.1103/PhysRevD.103.124012> for calculating both the linear perturbations to the general relativistic PR effect equations framed in the Kerr equatorial plane in the low luminosity limit, and the ratio of the Lyapunov timescale over the PR timescale in order to understand how the chaotic behavior impacts on the general relativistic PR dynamics.
- [56] W. H. Press, S. A. Teukolsky, W. T. Vetterling, and B. P. Flannery, *Numerical Recipes in C++: The Art of Scientific Computing* (2002), <http://adsabs.harvard.edu/abs/2002nrca.book.....P>.
- [57] V. De Falco, [arXiv:1904.01013](https://arxiv.org/abs/1904.01013).
- [58] *The Physics of Accretion onto Black Holes*, edited by M. Falanga, T. Belloni, P. Casella, M. Gilfanov, P. Jonker, and A. King (Springer-Verlag, New York, 2015).
- [59] M. Middleton, Black hole spin: Theory and observation, in *Astrophysics of Black Holes: From Fundamental Aspects to Latest Developments*, Astrophysics and Space Science Library, Vol. 440, edited by C. Bambi (Springer Berlin Heidelberg, Berlin, Heidelberg, 2016), p. 99.
- [60] J. Frank, A. King, and D. J. Raine, *Accretion Power in Astrophysics*, edited by J. Frank, A. King, and D. Raine (Cambridge University Press, Cambridge, England, 2002), pp. 398. ISBN 0521620538.
- [61] P. Bakala, M. Urbanec, E. Šrámková, Z. Stuchlík, and G. Török, *Classical Quantum Gravity* **29**, 065012 (2012).
- [62] N. R. Ikhsanov, *Astron. Astrophys.* **367**, 549 (2001).
- [63] A. González-Galán, E. Kuulkers, P. Kretschmar, S. Larsson, K. Postnov, A. Kochetkova, and M. H. Finger, *Astron. Astrophys.* **537**, A66 (2012).
- [64] H. Quaintrell, A. J. Norton, T. D. C. Ash, P. Roche, B. Willems, T. R. Bedding, I. K. Baldry, and R. P. Fender, *Astron. Astrophys.* **401**, 313 (2003).
- [65] R. M. Ludlam, J. M. Miller, D. Barret, E. M. Cackett, B. M. Coughenour, T. Dauser, N. Degenaar, J. A. García, F. A. Harrison, and F. Paerels, *Astrophys. J.* **873**, 99 (2019).
- [66] A. Niedźwiecki, *Mon. Not. R. Astron. Soc.* **356**, 913 (2005).
- [67] M. Gaspari, M. Ruzskowski, and S. P. Oh, *Mon. Not. R. Astron. Soc.* **432**, 3401 (2013).
- [68] A. King and C. Nixon, *Mon. Not. R. Astron. Soc.* **453**, L46 (2015).
- [69] P. Suková, M. Grzedzielski, and A. Janiuk, *Astron. Astrophys.* **586**, A143 (2016).
- [70] A. A. Blinova, M. M. Romanova, and R. V. E. Lovelace, *Mon. Not. R. Astron. Soc.* **459**, 2354 (2016).